Inorganic Chemistry
Article

Inorg. Chem. **2009**, *48*, 10371–10382 **10371**
DOI: 10.1021/ic9015959

Guided Ion Beam and Theoretical Studies of the Reactions of Pd^+ with CS_2: Thermochemistry of PdS^+ and $PdCS^+$

P. B. Armentrout*

Department of Chemistry, University of Utah, 314 S. 1400 E. Rm 2020, Salt Lake City, Utah 84112

Ilona Kretzschmar

Department of Chemical Engineering, The City College of New York, New York, New York 10031

Received August 10, 2009

The gas-phase reactivity of the atomic palladium cation with CS_2 is investigated using guided-ion beam mass spectrometry. Endothermic reactions forming PdS^+ and $PdCS^+$ are observed. Analysis of the kinetic energy dependence of the cross sections for formation of the two products yields the 0 K bond energies of $D_0(Pd^+-S) = 2.36 \pm 0.11$ eV and $D_0(Pd^+-CS) = 2.67 \pm 0.21$ eV. Quantum chemical calculations are used to investigate the electronic structure of the two product ions. In addition, detailed calculations of the potential energy surfaces reveal that the mechanism involves oxidative addition of a CS bond to the metal cation followed by simple bond cleavages. Formation of the ground-state PdS^+ ($^4\Sigma^-$) product is spin-forbidden from ground-state Pd^+ (^{2}D) whereas $PdCS^+$ ($^2\Sigma^+$) formation is spin-allowed. Crossing points between the doublet and quartet surfaces are located in the region of the $SPd^+(CS)$ intermediate, which suggests that coupling between the surfaces is efficient, consistent with experimental indications.

Introduction

Second-row transition-metal sulfides are useful as industrial catalysts[1,2] and semiconductor materials.[3] In particular, palladium sulfide is an expensive, but very active catalyst for desulfurization and hydrogenation processes.[4,5] Gas-phase hydrogenation of thiophene and its derivatives, for example, is an essential step in oil hydrotreating, and palladium sulfide catalysts, both supported and unsupported, are the most active catalysts for the reaction.[6,7] There is even a patent on the hydrogenation of CO with H_2 in the presence of a metal sulfide catalyst, which contains palladium and one promoter alkali metal, alkaline earth metal, or rare earth element.[8] Further, palladium sulfide is used as a catalyst for electrolytic plating because it shows good long-term stability (months vs days), high plating coverage, and low resistivity.[9] Palladium sulfide has also been employed because of its semiconducting properties[10] as (i) low-resistance ohmic contacts in semiconducting electronic devices, (ii) light image receiving material, (iii) photographic films, (iv) lithographic plates and films, and (v) embedded in a polymer matrix for solar cells. In addition, studies reveal that PdS thin films are a good alternative for solar applications because of the direct interband transition ($E_g = 1.60 \pm 0.01$ eV), the high optical absorption coefficient (10^5 cm^{-1}) at energies above 2.0 eV, the observed n-type conductivity, and the adequate donor density.[11] More recently, palladium sulfide has received

*To whom correspondence should be addressed. E-mail: armentrout@chem.utah.edu.

(1) (a) Fărcaşiu, D.; Ghenciu, A.; Li, J. Q. *J. Catal.* **1996**, *158*, 116. (b) Raje, A. P.; Liaw, S.-J.; Srinivasan, R.; Davis, B. H. *Appl. Catal., A* **1997**, *150*, 297. (c) Allali, N.; Prouzet, E.; Michalowicz, A.; Gaborit, V.; Nadiri, A.; Danot, M. *Appl. Catal., A* **1997**, *159*, 333. (c) Mdleleni, M. M.; Hyeon, T.; Suslick, K. S. *J. Am. Chem. Soc.* **1998**, *120*, 6189. (d) Dos Santos, A. C. B.; Grange, P.; Faro, A. C., Jr. *Appl. Catal., A* **1999**, *178*, 29. (e) Janssens, J.-P.; van Langeveld, D. A.; Moulijn, J. A. *Appl. Catal., A* **1999**, *179*, 229.

(2) For a comparison of hydrodechlorination and hydrodesulfurization selectivities and activities of MS (M = V−Ni; Mo−Pd, W, Ir, Pt), see: Frimmel, J.; Zaradzil, M. *J. Catal.* **1997**, *167*, 286.

(3) See, for example: (a) Dusheiko, V. A.; Lipkin, M. S. *J. Power Source* **1995**, *54*, 264. (b) Smith, P. R.; Holmes, J. D.; Richardson, D. J.; Russell, D. A.; Sodeau, J. R. *J. Chem. Soc., Faraday Trans.* **1998**, *94*, 1235. (c) Lifshitz, E.; Litvin, I. D.; Porteanu, H.; Lipovskii, A. A. *Chem. Phys. Lett.* **1998**, *295*, 249.

(4) Dolbeer, G. E. *Hydrocracking: Reactions, Catalysts, and processes in Petroleum Chemistry and Refining*; Speight, J. G., Ed.; Taylor & Francis: Washington, DC, 1998; Chapter 7, pp 175.

(5) Dey, S.; Jain, V. K. *Platinum Met. Rev.* **2004**, *48*, 16–29.

(6) Mashkina, A. V.; Zirka, A. A. *Kinet. Catal.* **2000**, *41*, 575–581.

(7) Ermakova, A.; Mashkina, A.; Sakhaltueva, L. G. *Kinet. Catal.* **2002**, *43*, 528–535.

(8) *Hydrogenation of carbon monoxide using sulfide catalysts*. U.S. Patent US6534553.

(9) Bladon, J. J.; Lamola, A.; Lytle, F. W.; Sonnenberg, W.; Robinson, J. N.; Philipose, G. *J. Electrochem. Soc.* **1996**, *143*, 1206–1213.

(10) Dey, S.; Jain, V. K. *Platinum Met. Rev.* **2004**, *48*, 16–29.

(11) Ferrer, I. J.; Díaz-Cao, P.; Pascual, A.; Sánchez, C. *Thin Solid Films* **2007**, *515*, 5783–5786.

Published on Web 10/02/2009

attention as a possible material for nanoparticle synthesis. Palladium sulfide nanoparticles with diameters of 4.87 ± 0.49 nm[12] and 2.87 ± 0.51 nm[13] have been synthesized, and PdS_x is a key material for the growth of anisotropic heterostructures, for example, novel peanut-shaped Pd−Co−Pd sulfide nanoparticles.[14] Researchers have also found that the Pd−S bond of thiol-capped Pd clusters exhibiting room temperature magnetism contributes to the magnetic moment by increasing the density of holes at the 4d residual band of the Pd nanoparticle.[15] In addition, the thermochemistry[16] and solubility[17] of palladium sulfide are of geological importance as the aqueous transport of platinum-group elements from naturally occurring minerals such as vysotskite (PdS) during high-temperature geochemical processes has been suggested. The thermochemistry of palladium sulfides has been studied and a standard molar enthalpy of formation of $\Delta_f H_m°$ (PdS, 298.15 K) = (−78.1 ± 11.0 kJ/mol)[18] has been determined in good agreement with an earlier compilation of Mills.[19] Despite the utility of PdS, only a few temperature solubility studies of PdS(s) have been performed and have been found to be either inconclusive or unreliable.[20] No gas-phase studies have been performed on palladium sulfides and are needed to shed light on their thermodynamic properties.

In previous work, we have investigated the gas-phase thermodynamic properties of the sulfides of first-row[21−29] and several early second-row[29,30] transition-metal cations, as well as reviewed the periodic trends in this information.[31] In the present study, we investigate the gas-phase thermodynamic properties of the sulfide of one of the late metals of the second transition row, palladium, which augments parallel studies of ruthenium,[32] rhodium,[33] and silver.[34] The reactions of the atomic cations of palladium with carbon disulfide, CS_2, have previously been studied at room temperature in a high pressure of He by Bohme and co-workers,[35] who observed only $Pd^+(CS_2)$ adduct formation. In the present work, the reaction of Pd^+ with CS_2 is studied under single collision conditions using guided-ion beam (GIB) mass spectrometric (GIBMS) techniques. The endothermic reactions 1 and 2 are both observed, and their dependence on kinetic energy is measured.

$$Pd^+ + CS_2 \rightarrow PdS^+ + CS \quad (1)$$

$$\rightarrow PdCS^+ + S \quad (2)$$

An analysis of the kinetic energy dependence permits the endothermicities of reactions 1 and 2 to be measured and converted to the 0 K bond dissociation energies, $D_0(Pd^+-S)$ and $D_0(Pd^+-CS)$. Quantum-chemical methods are employed to complement the thermodynamic data with information on electronic ground and low-lying excited states, bond lengths, and vibrational frequencies of PdS^+ and $PdCS^+$. Additional calculations reveal the mechanism for the reaction by exploring the potential energy surfaces for several spin states of the reactants.

Experimental and Computational Methods

Experimental Approach. GIB mass spectrometry is used for the evaluation of thermodynamic data by means of threshold measurements of endothermic reactions. Detailed descriptions of the GIB apparatus used in this study and the experimental procedures are given elsewhere.[36,37] Briefly, Ar^+ ions created in a direct current (DC) discharge source[37] are accelerated toward a palladium cathode thereby sputtering off Pd^+ ions. The metal ions drift in a meter-long flow tube operated with a 9:1 mixture of helium and argon at a pressure of ∼90 Pa. The ions undergo $\sim 10^5$ collisions with the buffer gas before exiting the flow tube, and therefore are expected to equilibrate to room temperature.[38,39] Previous studies of the reactions of Pd^+ formed in this source showed no indications of excited states;[38,40,41] however, as shown below, excited states are found in the present work, showing that full equilibration has not occurred. To try to quench these excited states, about 0.7 Pa of carbon disulfide is introduced about 25 cm downstream from the discharge. Operation at these pressures allows the ions to undergo 10^2-10^3 collisions with CS_2 molecules in the flow tube, which reduces the excited state population but does not remove it, as shown below. Therefore, data for reaction of ground-state ions shown below are obtained by extrapolating the features in the cross sections attributable to excited states to zero, as detailed below. Addition of methane to the flow tube, used successfully to quench excited states of several other

(12) Malik, M. A.; O'Brien, P.; Revaprasadu, N. *J. Mater. Chem.* **2002**, *12*, 92–97.
(13) Yang, Z.; Smetana, A. B.; Sorensen, C. M.; Klabunde, K. J. *Inorg. Chem.* **2007**, *46*, 2427–2431.
(14) Teranishi, T.; Saruyama, M.; Nakaya, M.; Kanehara, M. *Angew. Chem., Int. Ed.* **2007**, *46*, 1713–1715.
(15) Hernando, A.; Sampedro, B.; Litrán, R.; Rojas, T. C.; Sánchez-López, J. C.; Fernández, A. *Nanotechnology* **2006**, *17*, 1449–1453.
(16) Sassani, D. C.; Shock, E. L. *Geochim. Cosmochim. Acta* **1998**, *62*, 2643–2671.
(17) Pan, P.; Wood, S. A. *Mineral. Deposita* **1994**, *29*, 373–390.
(18) Zubkov, A.; Fujino, T.; Sato, N.; Yamada, K. *J. Chem. Thermodyn.* **1998**, *30*, 571–581.
(19) Mills, K. S. *Thermodynamic Data for Inorganic Sulphides, Selenides and Tellurides*; Butterworths: London, 1974; pp 522−524.
(20) Hummel, W.; Berner, U.; Curti, E.; Pearson, F. J.; Thoenen, T. *Nagra/PSI Chemical Thermodynamic Data Base 01/01* Universal Publisher: U.S.A., 2002; pp 248−252.
(21) Kretzschmar, I.; Schröder, D.; Schwarz, H.; Rue, C.; Armentrout, P. B. *J. Phys. Chem. A* **1998**, *102*, 10060–10073.
(22) Rue, C.; Armentrout, P. B.; Kretzschmar, I.; Schröder, D.; Harvey, J. N.; Schwarz, H. *J. Chem. Phys.* **1999**, *110*, 7858–7870.
(23) Schröder, D.; Kretzschmar, I.; Schwarz, H.; Rue, C.; Armentrout, P. B. *Inorg. Chem.* **1999**, *38*, 3474–3480.
(24) Bärsch, S.; Kretzschmar, I.; Schröder, D.; Schwarz, H.; Armentrout, P. B. *J. Phys. Chem. A* **1999**, *103*, 5925–5934.
(25) Kretzschmar, I.; Schröder, D.; Schwarz, H.; Rue, C.; Armentrout, P. B. *J. Phys. Chem. A* **2000**, *104*, 5046–5058.
(26) Kretzschmar, I.; Schröder, D.; Schwarz, H. *J. Phys. Chem. A* **2001**, *105*, 8456–8464.
(27) Rue, C.; Armentrout, P. B.; Kretzschmar, I.; Schröder, D.; Schwarz, H. *Int. J. Mass Spectrom.* **2001**, *210/211*, 283–301.
(28) Rue, C.; Armentrout, P. B.; Kretzschmar, I.; Schröder, D.; Schwarz, H. *J. Phys. Chem. A* **2002**, *106*, 9788–9797.
(29) Kretzschmar, I.; Schröder, D.; Schwarz, H.; Armentrout, P. B. *Int. J. Mass Spectrom.* **2003**, *228*, 439–456.
(30) Kretzschmar, I.; Schröder, D.; Schwarz, H.; Armentrout, P. B. *Int. J. Mass Spectrom.* **2006**, *249−250*, 263–278.
(31) Kretzschmar, I.; Schröder, D.; Schwarz, H.; Armentrout, P. B. *Advances in Metal and Semiconductor Clusters*; Duncan, M. A., Ed.; JAI Press: Greenwich, CT, 2001; Vol. *5*, pp 347−394.
(32) Armentrout, P. B.; Kretzschmar, I.; work in progress.
(33) Armentrout, P. B.; Kretzschmar, I. *J. Phys. Chem. A*, **2009**, in press.
(34) Armentrout, P. B.; Kretzschmar, I. *J. Chem. Phys.*, submitted for publication.
(35) Cheng, P.; Koyanagi, G. K.; Bohme, D. K. *J. Phys. Chem. A* **2006**, *110*, 2718–2728.
(36) Ervin, K. M.; Armentrout, P. B. *J. Chem. Phys.* **1985**, *83*, 166.
(37) Schultz, R. H.; Armentrout, P. B. *Int. J. Mass Spectrom. Ion Processes* **1991**, 107 29.
(38) Chen, Y.-M.; Elkind, J. L.; Armentrout, P. B. *J. Phys. Chem.* **1995**, *99*, 10438–10445.
(39) Sievers, M. R.; Chen, Y.-M.; Elkind, J. L.; Armentrout, P. B. *J. Phys. Chem.* **1996**, *100*, 54–62.
(40) Chen, Y.-M.; Armentrout, P. B. *J. Chem. Phys.* **1995**, *103*, 618–625.
(41) Chen, Y.-M.; Sievers, M. R.; Armentrout, P. B. *Int. J. Mass Spectrom. Ion Processes* **1997**, *167/168*, 195–212.

metal cations,[32,33] is found to have no effect on the cross sections observed for Pd^+.

Following extraction from the source, the ions are accelerated and focused into a magnetic sector, mass-selected, decelerated to a desired kinetic energy, and focused into an octopole ion trap.[36,42] The ion trap guides the ions through a static gas cell kept at a low pressure (0.01−0.03 Pa) of the reactant gas. It is verified that all product cross sections reported result from single ion−molecule collisions by examining the pressure dependence of the product intensities. After exiting the gas cell, product and remaining reactant ions drift to the end of the octopole where they are directed into a quadrupole mass filter for mass analysis and then detected. Conversion of the raw ion intensities into reaction cross sections and the conversion from the laboratory to center-of-mass energy scale are treated as described previously.[36] Retarding potential measurements are used to determine the distribution and absolute zero of the ion kinetic energy. The accuracy of the absolute cross sections is estimated to be ± 20%. The beams have Gaussian kinetic energy distributions with average full widths at half-maximum (fwhm) of about 0.25 eV in the laboratory frame. The uncertainty of the absolute energy scale is ± 0.05 eV (lab).

Data Analysis. Quantitative analysis of the energy dependence of these cross sections is achieved using eq 3 and methods outlined elsewhere.[43−47]

$$\sigma(E) = \sigma_0 \sum g_i (E + E_i - E_0)^n / E^m \quad (3)$$

In eq 3, E is the relative kinetic energy of the reactants, E_0 is the threshold for reaction at 0 K, σ_0 is a scaling parameter, and n and m are fitting parameters describing the energy dependence. The summation is over the rovibrational states of the reactants having energies E_i and populations g_i ($\Sigma g_i = 1$) with molecular parameters for CS_2 taken from B3LYP/Def2TZVPP calculations performed here for consistency. (Vibrational frequencies agree with experiment[48] within 3%, and the rotational constants are the same.)

In addition to modeling the reaction product cross sections independently using eq 3, we also examine competition between the two reaction channels by using a statistical approach that has been described in detail elsewhere,[49,50] eq 4.

$$\sigma_j(E) = (n\sigma_{0,j}/E^m) \sum g_i \int_{E_{0,j}-E_i}^{E} [k_j(E^*)/k_{tot}(E^*)] [1 - e^{k_{tot}(E^*)\tau}](E - \varepsilon)^{n-1} \, d(\varepsilon) \quad (4)$$

Here $\sigma_{0,j}$ is a scaling parameter for channel j that is energy independent, $E_{0,j}$ represents the threshold energy for channel j at 0 K, ε is the energy available from reactant translation, and τ is the experimental time for dissociation. E^* is the internal energy of the energized molecule (EM), that is, $E^* = \varepsilon + E_i$. The term $k_j(E^*)$ is the unimolecular rate constant for dissociation of the EM to channel j. The rate constants $k_j(E^*)$ and $k_{tot}(E^*)$ are defined by Rice−Ramsperger−Kassel−Marcus (RRKM)[51−53] theory in eq 5,

$$k_{tot}(E^*) = \sum k_j(E^*) = \sum d_j N_{j,vr}(E^* - E_{0,j})/h\rho_{vr}(E^*) \quad (5)$$

where d_j is the reaction degeneracy for channel j, h is Planck's constant, $N^{\dagger}_{j,vr}(E^*-E_{0,j})$ is the sum of rovibrational states of the transition state (TS) at an energy $E^* - E_{0,j}$ for channel j, and $\rho_{vr}(E^*)$ is the density of rovibrational states of the EM at the available energy, E^*. Transition states for both reaction channels are treated as loose transition states at the phase space limit (PSL),[49] in which case molecular parameters for the EM and TSs are taken from the quantum chemical calculations described below. Because formation of $PdCS^+ + S$ corresponds to a covalent bond cleavage from the presumed intermediate, we also considered whether a tight transition state might be more appropriate, as this has been found for other systems involving covalent bonds.[54,55] Here, the molecular parameters of the transition state are equated with those of the EM after removing the reaction coordinate, that is, the Pd−S stretch. This is the tightest realistic transition state for a bond cleavage reaction that has no barrier along the dissociation coordinate, as verified by quantum calculations for reaction 2. In these models, the adiabatic 2-D rotational energy is treated using a statistical distribution with explicit summation over the possible values of the rotational quantum number, as described in detail elsewhere.[49]

Before comparison with the data, eqs 3 and 4 are convoluted over the translational energy distributions of both reactants. This determination of the reaction thresholds involves explicit consideration of the distributions of vibrational, rotational, and translational energies of both reactants. Because all sources of reactant energy are considered, the thermochemistry obtained corresponds to 0 K values in all cases.

Theoretical Approach. The bond lengths and the ground state/excited state splittings of PdS^+ and $PdCS^+$ are calculated with density functional theory (DFT). Preliminary DFT calculations were carried out using the Amsterdam density functional (ADF, version 2.0.1) suite of programs[56] with the inner-shell electrons ([Ne] for S and [Ar] for Pd) treated in the frozen-core approximation.[57] The valence orbitals are expanded as linear combinations of Slater-type basis functions. Triple-zeta basis

(42) Gerlich, D. *Adv. Chem. Phys.* **1992**, *82*(Part 1), 1–176.
(43) Chesnavich, W. J.; Bowers, M. T. *J. Phys. Chem.* **1979**, *83*, 900–905.
(44) Aristov, N.; Armentrout, P. B. *J. Am. Chem. Soc.* **1986**, *108*, 1806–1819.
(45) Schultz, R. H.; Crellin, K. C.; Armentrout, P. B. *J. Am. Chem. Soc.* **1991**, *113*, 8590.
(46) Armentrout, P. B. In *Advances in Gas Phase Ion Chemistry*; Adams, N. G., Babcock, L. M., Eds.; JAI Press: Greenwich, 1992; Vol. *1*, pp 83-119.
(47) Armentrout, P. B. *Int. J. Mass Spectrom.* **2000**, *200*, 219–241.
(48) Herzberg, G. *Molecular Spectra and Molecular Structure*; Van Nostrand Reinhold: New York, 1966; Vol. *III*.
(49) Rodgers, M. T.; Ervin, K. M.; Armentrout, P. B. *J. Chem. Phys.* **1997**, *106*, 4499.
(50) Rodgers, M. T.; Armentrout, P. B. *J. Chem. Phys.* **1998**, *109*, 1787.
(51) Gilbert, R. G.; Smith, S. C. *Theory of Unimolecular and Recombination Reactions*; Blackwell Scientific: London, 1990.
(52) Truhlar, D. G.; Garrett, B. C.; Klippenstein, S. J. *J. Phys. Chem.* **1996**, *100*, 12771.
(53) Holbrook, K. A.; Pilling, M. J.; Robertson, S. H. *Unimolecular Reactions*, 2nd ed.; Wiley: New York, 1996.
(54) Muntean, F.; Heumann, L.; Armentrout, P. B. *J. Chem. Phys.* **2002**, *116*, 5593.
(55) Muntean, F.; Armentrout, P. B. *J. Phys. Chem. A.* **2003**, *107*, 7413.
(56) te Velde, G.; Baerends, E. J. *ADF*; Department of Theoretical Chemistry, Vrije Universiteit: Amsterdam, The Netherlands.
(57) Snijders, J. G.; Baerends, E. *J. Mol. Phys.* **1977**, *33*, 1651.
(58) Vosko, S. H.; Wilk, L.; Nusair, M. *Can. J. Phys.* **1980**, *58*, 1200.
(59) Becke, A. D. *Phys. Rev. A* **1988**, *38*, 3098.
(60) Perdew, J. P. *Phys. Rev. B* **1986**, *33*, 8822.
(61) Levy, M.; Perdew, J. P. *Int. J. Quantum Chem.* **1994**, *49*, 539.
(62) Frisch, M. J.; Trucks, G. W.; Schlegel, H. B.; Scuseria, G. E.; Robb, M. A.; Cheeseman, J. R.; Montgomery, J., J. A. ; Vreven, T.; Kudin, K. N.; Burant, J. C.; Millam, J. M.; Iyengar, S. S.; Tomasi, J.; Barone, V.; Mennucci, B.; Cossi, M.; Scalmani, G.; Rega, N.; Petersson, G. A.; Nakatsuji, H.; Hada, M.; Ehara, M.; Toyota, K.; Fukuda, R.; Hasegawa, J.; Ishida, M.; Nakajima, T.; Honda, Y.; Kitao, O.; Nakai, H.; Klene, M.; Li, X.; Knox, J. E.; Hratchian, H. P.; Cross, J. B.; Adamo, C.; Jaramillo, J.; Gomperts, R.; Stratmann, R. E.; Yazyev, O.; Austin, A. J.; Cammi, R.; Pomelli, C.; Ochterski, J. W.; Ayala, P. Y.; Morokuma, K.; Voth, G. A.; Salvador, P.; Dannenberg, J. J.; Zakrzewski, V. G.; Dapprich, S.; Daniels, A. D.; Strain, M. C.; Farkas, O.; Malick, D. K.; Rabuck, A. D.; Raghavachari, K.; Foresman, J. B.; Ortiz, J. V.; Cui, Q.; Baboul, A. G.; Clifford, S.; Cioslowski, J.; Stefanov, B. B.; Liu, G.; Liashenko, A.; Piskorz, P.; Komaromi, I.; Martin, R. L.; Fox, D. J.; Keith, T.; Al-Laham, M. A.; Peng, C. Y.; Nanayakkara, A.; Challacombe, M.; Gill, P. M. W.; Johnson, B.; Chen, W.; Wong, M. W.; Gonzalez, C.; Pople, J. A. *Gaussian 03*, Revision B.02; Gaussian, Inc.: Pittsburgh, PA, 2003.

sets are used for palladium and sulfur. All molecular and atomic energies are calculated using the local spin density approximation (LDA) with Slater's exchange functional and the Vosko−Wilk−Nusair parametrization (VWN)[58] augmented by Becke's[59] and Perdew's[60] (BP) gradient corrections for the exchange and correlation potentials, respectively.[61] This method will be referred to as ADF/BP. Particular advantages of the ADF program are that it provides control over the symmetry of the wave function created during geometry optimizations and permits the calculations of excited states.

Using these geometries as starting points, we perform calculations using the Gaussian 03 suite of programs[62] with the B3LYP hybrid density functional method[63,64] and Def2TZVPP basis sets, which are balanced basis sets of triple-ζ valence quality, with contracted basis functions of [5s3p2d1f] for C, [5s5p3d1f] for S, and [6s4p3d2f1g] for Pd.[65,66] The Def2TZVPP basis set for Pd uses a small core (28 electron) effective core potential (ECP) developed by Andrae et al.[67] These basis sets were obtained from the EMSL basis set library.[68,69] Geometries and relative energies found at the B3LYP/Def2TZVPP level of theory are comparable to those found for the ADF/BP level; hence the latter results are not reported below in particular because the ADF program is not designed to assess accurate bond energies. In addition, to provide more accurate thermodynamic information, we also calculate single point energies of Pd^+, S, CS, CS_2, PdS^+, and $PdCS^+$ at the CCSD(T)/Def2TZVPP level of theory[70,71] using B3LYP/Def2TZVPP geometries and zero point energy corrections. The CCSD(T)/Def2TZVPP//B3LYP/Def2TZVPP level of theory is also used to examine the potential energy surfaces for the reactions. In all cases reported below, the single point energies cited include zero point energy corrections using unscaled B3LYP/Def2TZVPP vibrational frequencies. Finally, geometry optimizations at the CCD/Def2TZVPP (chosen because of the availability of analytic gradients) and CCSD(T) levels of theory are performed on the ground states of PdS^+ and $PdCS^+$ to examine the dependence of the structures on the level of theory. Because the results presented below generally involve only the Def2TZVPP basis set, they will usually be distinguished only by the level of theory used.

The thermodynamic accuracy of these results can be assessed by comparing them to several well-known thermodynamic quantities. At the CCSD(T) (B3LYP) levels of theory, C−S and S−CS bond energies are calculated to be 7.05 (7.14) and 4.35 (4.70) eV, respectively. These energies compare well with the experimental bond energies of 7.37 ± 0.04 eV and 4.50 ± 0.04 eV, respectively.[72] Likewise, the average excitation energies of different spin states of Pd^+ are reproduced reasonably well. Experiment finds a $^2D(4d^9)$ ground state for Pd^+, with a $^4F(5s^14d^8)$ state at 3.194 eV (average over all spin−orbit levels of both states).[73] The two levels of theory find a ^2D ground state and yield values of 3.01 (2.96) eV for the ^4F state excitation energy.

Theoretical Results

To fully understand the experimental results, it is important to know the nature of the electronic states of the product PdS^+ and $PdCS^+$ species, along with the potential energy surfaces for reaction. The following sections contain these theoretical results as obtained using the computational procedures described above.

Table 1. Bond Lengths, Vibrational Frequencies, and State Splittings for PdS^+[a]

state	r, Å	ν, cm^{-1}	E_{rel} (B3LYP), eV[b]	E_{rel} (CCSD(T)), eV[b]
$^4\Sigma^-$	2.133, **2.265**, *2.112*	393, **252**	0.000	0.000, **0.000**, *0.000*
$^2\Sigma^-$	2.141, **2.327**, *2.143*	375, **239**	0.235	0.296, **0.299**, *0.300*
$^4\Delta$	2.301	299	0.945	0.856
$^2\Delta$	2.331	279	1.028	0.927
$^2\Pi$	2.190	229	1.112	0.931
$^2\Pi$	2.152	386	1.166	0.964
$^4\Phi$	2.312	292	1.764	1.647

[a] Geometry optimizations and frequency calculations performed at the B3LYP/Def2TZVPP, CCD/Def2TZVPP (bold), CCSD(T)/Def2TZVPP (italics) levels of theory. [b] Relative single point energies calculated at the indicated level of theory and corrected for zero point energies.

PdS^+. At the B3LYP/Def2TZVPP level of theory, calculations predict a $^4\Sigma^-$ ground state for PdS^+. The ground state valence electron configuration is $(1\sigma)^2(2\sigma)^2(1\pi)^4(1\delta)^4(3\sigma)^1(2\pi)^2$ where the 1σ orbital is largely S(3s), the 2σ and 1π orbitals are the metal−sulfur bonding orbitals, the 1δ are Pd(4d), the 3σ is largely Pd(5s), and 2π and 4σ are antibonding orbitals. Bond lengths calculated at the B3LYP and CCSD(T) level are similar to one another, with the CCD result being longer by over 0.1 Å. A $^2\Sigma^-$ state having the same electron configuration (with the 3σ electron low-spin coupled to the 2π electrons) is found only 0.23−0.30 eV higher in energy, Table 1. This state has a slightly longer bond length than the ground state, with similar variations among the three levels of theory. Between 0.8 and 1.2 eV above the ground state, a $^4\Delta$, $^2\Delta$, and two $^2\Pi$ states are located. The two Δ states have $(1\sigma)^2(2\sigma)^2(1\pi)^4(1\delta)^3(3\sigma)^2(2\pi)^2$ configurations (with the 1δ electron either high-spin or low-spin coupled to the 2π electrons), whereas the Π states have $(1\sigma)^2(2\sigma)^2(1\pi)^4(1\delta)^4(3\sigma)^2(2\pi)^1$ and $(1\sigma)^2(2\sigma)^2(1\pi)^4(1\delta)^4(3\sigma)^0(2\pi)^3$ configurations. A $^4\Phi$ state with a $(1\sigma)^2(2\sigma)^2(1\pi)^4(1\delta)^3(3\sigma)^1(2\pi)^3$ configuration is located 1.65−1.76 eV above the ground state. The Σ and Π states, which have bond lengths of 2.13−2.19 Å, have three electrons in the 3σ or 2π orbitals. In contrast, the $^4\Delta$, $^2\Delta$, and $^4\Phi$ states have longer bond lengths of 2.30−2.33 Å because they have 4 electrons in the antibonding 3σ and 2π orbitals. Vibrational frequencies follow these trends as well, ~390 and 290 cm^{-1} for the two groups, respectively, except for the lower-lying $^2\Pi$ state, which has a frequency of 229 cm^{-1} because of its $3\sigma^2$ occupation. In all cases, the states adiabatically correlate with $Pd^+(^2D) + S(^3P)$ separated atoms.

The excitation energy of the low-lying $^2\Sigma^-$ state relative to the $^4\Sigma^-$ state might be influenced by the relative energies of the ^2D and ^4F states of Pd^+, where B3LYP and CCSD(T) theory find ^4F excitation energies that lie 0.23 and 0.18 eV, respectively, below the experimental value (see above). If these differences are used to correct the molecular excitation energies, then the relative energy of the $^2\Sigma^-$ state drops to 0.001 and 0.11 eV for the B3LYP and CCSD(T)//B3LYP levels of theory, respectively.

$PdCS^+$. The ground state of palladium thiocarbonyl cation is calculated to be a $^2\Sigma^+$ state corresponding to

(63) Becke, A. D. *J. Chem. Phys.* **1993**, *98*, 5648–5652.
(64) Lee, C.; Yang, W.; Parr, R. G. *Phys. Rev. B* **1988**, *37*, 785–789.
(65) Eichkorn, K.; Weigend, F.; Treutler, O.; Ahlrichs, R. *Theor. Chem. Acc.* **1997**, *97*, 119.
(66) Weigend, F.; Ahlrichs, R. *Phys. Chem. Chem. Phys.* **2005**, *7*, 3297.
(67) Andrae, D.; Haeussermann, U.; Dolg, M.; Stoll, H.; Preuss, H. *Theor. Chim. Acta* **1990**, *77*, 123–141.
(68) Feller, D. *J. Comput. Chem.* **1996**, *17*, 1571–1586.
(69) Schuchardt, K. L.; Didier, B. T.; Elsethagen, T.; Sun, L.; Gurumoorthi, V.; Chase, J.; Li, J.; Windus, T. L. *J. Chem. Inf. Model.* **2007**, *47*, 1045.
(70) Cizek, J. *Adv. Chem. Phys.* **1969**, *14*, 35–89.
(71) Purvis, G. D. I.; Bartlett, R. J. *J. Chem. Phys.* **1982**, *76*, 1910.
(72) Prinslow, D. A.; Armentrout, P. B. *J. Chem. Phys.* **1991**, *94*, 3563.
(73) Litzén, U.; Lundberg, H.; Tchang-Brillet, W.-U. L.; Launay, F.; Engleman, R., Jr. *Phys. Scr.* **2001**, *64*, 63.

Table 2. Bond Lengths, Bond Angles, Vibrational Frequencies, and State Splittings for CS and $PdCS^{+a}$

species	state	r(Pd−C), Å	r(C−S), Å	∠PdCS, deg	ν, cm^{-1}	E_{rel}, eV^b
CS	$^1\Sigma^+$		1.532		1311	0.000 (0.000)
			1.527		**1362**	
			1.544			
$Pd^+(CS)$	$^2\Sigma^+$	1.904	1.503	180.0	247 (2), 330, 1451	0.000 (0.000)
		1.987	**1.470**	**180.0**		
		1.918	*1.506*	*180.0*		
	$^2\Delta$	2.030	1.501	180.0	212 (2), 280, 1460	0.054 (0.780)
	$^2\Pi$	2.116	1.501	180.0	180, 196, 235, 1426	0.890 (1.033)
	$^4A'$	1.884	1.634	142.6	121, 449, 989	3.759 (3.455)
	$^4\Sigma(^4A'')$	1.868	1.643	180.0	−183, 190, 337, 1012	4.230 (3.930)

[a] Geometry optimizations and frequency calculations performed at B3LYP/Def2TZVPP, CCD/Def2TZVPP (bold), CCSD(T)/Def2TZVPP (italics) levels of theory. [b] Relative single point energies calculated at CCSD(T)/Def2TZVPP (B3LYP/Def2TZVPP) levels of theory and corrected for zero point energies.

binding of CS to the ^2D ground state of Pd^+ with the electron hole in the 4dσ orbital (the 4d orbital pointed along the bonding axis). As shown in Table 2, the CS bond length in ground-state $PdCS^+$ is slightly shorter than in free CS, 1.503 versus 1.532 Å (1.470 versus 1.527 Å at the CCD level of theory and 1.506 vs 1.544 Å at the CCSD(T) level of theory). Consistent with this observation, the vibrational frequency of the CS bond stretch increases from 1311 cm^{-1} to 1451 cm^{-1}. The $PdCS^+$ molecule has a valence electron configuration of $(1\sigma)^2(2\sigma)^2(1\pi)^4(3\sigma)^2(2\pi)^4(1\delta)^4(4\sigma)^1$ where the 1σ, 2σ, and 1π orbitals are the carbon−sulfur bonding orbitals, the 3σ is a metal−carbon bond formed by donation of the highest occupied molecular orbital (HOMO) of CS into a 5s-4dσ hybrid on Pd, the 2π are the backbonding interactions between the metal 4dπ and the antibonding π orbitals on CS, the 1δ are Pd(4d), the 4σ is the other Pd(5s-4dσ) hybrid, and 3π and 5σ are antibonding orbitals. If the electron hole on Pd^+ is located in the δ or π orbital, $^2\Delta$ and $^2\Pi$, respectively, excited states are formed, Table 2. The excited states have electron configurations of $(1\sigma)^2(2\sigma)^2(1\pi)^4(3\sigma)^2(2\pi)^4(1\delta)^3(4\sigma)^2$ and $(1\sigma)^2(2\sigma)^2(1\pi)^4(3\sigma)^2(2\pi)^3(1\delta)^4(4\sigma)^2$, respectively, and longer Pd−C bond lengths of 2.030 and 2.116 Å, respectively, compared to the ground state, 1.904 Å. The CS stretching frequencies are similar for the $^2\Sigma^+$ and $^2\Delta$ states, ∼1455 cm^{-1}, but lower for $^2\Pi$ (1426 cm^{-1}) because there is less π backbonding in the latter state.

In contrast to the linear geometries of the doublet states, a $^4A'$ state has a bent geometry with a slightly shorter Pd−C bond length (1.884 Å) and a much lower CS bond stretch (989 cm^{-1}) than the $^2\Sigma^+$ ground state. The excitation energy of this state, 3.46−3.76 eV is similar to the ^2D−^4F excitation energy of atomic Pd^+. Using linear symmetry designations, the $^4A'$ state has a $(1\sigma)^2(2\sigma)^2(1\pi)^4(3\sigma)^2(2\pi)^4(1\delta)^3(4\sigma)^1(3\pi)^1$ configuration in which one of the antibonding 3π orbitals is singly occupied, which explains why the molecule is bent. A $^4\Sigma$ ($^4A''$) state with a $(1\sigma)^2(2\sigma)^2(1\pi)^4(3\sigma)^2(2\pi)^3(1\delta)^4(4\sigma)^1(3\pi)^1$ configuration is located at 3.93−4.23 eV, Table 2, but has an imaginary frequency of 183 cm^{-1} corresponding to a bending mode. Thus, this linear state will collapse to the lower-energy bent $^4A'$ state.

Doublet Potential Energy Surface. The reaction coordinate diagram for reaction of CS_2 with Pd^+ in the doublet and quartet spin states is shown in Figure 1. The energies used in this diagram are calculated at the CCSD(T)//B3LYP level of theory, and these values will

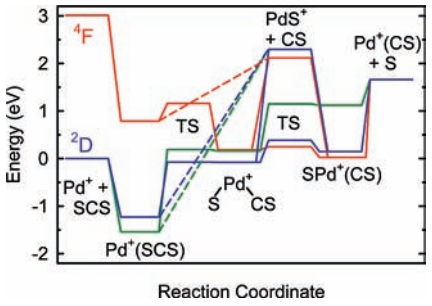

Figure 1. Reaction coordinate diagram for reaction of Pd^+ in doublet ($^2A''$, blue line; $^2A'$, green line) and quartet (red line) states with CS_2. All energies are calculated at the CCSD(T)//B3LYP level including zero point energies. Possible dissociations from bent $SPd^+(CS)$ to $Pd^+(CS)$ + S products are not explicitly indicated. Dashed lines show direct formation of PdS^+ + CS from the $Pd^+(SCS)$ intermediates.

be used throughout the following discussion. Geometries of intermediates and products of reactions 1 and 2 are shown in Figure 2 in the same order as one moves across Figure 1 with energies and structural parameters provided in Table 3. All of the species are planar with the exception of the $^4A''$ state of $Pd^+(SCS)$.

Along the doublet surface, the initial interaction of $Pd^+(^2D)$ with CS_2 leads to the $Pd^+(SCS)$ ($^2A'$) complex bound by 1.54 eV with respect to the reactants. The $Pd^+(SCS)$ species can be thought of as the donation of the nonbonding in-plane π electrons of CS_2 into the singly occupied 4dσ orbital on Pd^+ (where the latter undergoes s-d hybridization to minimize the repulsion). Therefore, the structure has a bent geometry with r(Pd−S) = 2.331 Å and ∠PdSC = 103°, Figure 2. In this complex, the CS_2 ligand is distorted by stretching the CS bond closer to the metal ion (and shortening the other CS bond) and bending the ligand to 176° from linear. A $^2A''$ state is located 0.31 eV higher in energy with a very similar geometry. Here, the singly occupied π-like orbital lies out of the plane of the molecule. Linear doublet (Σ, Π, and Δ) states are found at 0.88−0.98 eV above the $^2A'$ ground state, but these species all have imaginary bending motions that carry them to one of the lower-lying $^2A'$ or $^2A''$ structures.

From the encounter complex, reaction takes place by oxidative addition of a CS bond to the palladium center, leading to the transition state TS($^2A''$). The imaginary frequency of 175 cm^{-1} corresponds to elongation of the CS bond coordinated to Pd^+. The transition state has slightly longer PdS and PdC bond lengths and a smaller SPdC bond angle compared to the $SPd^+(CS)$ ($^2A''$)

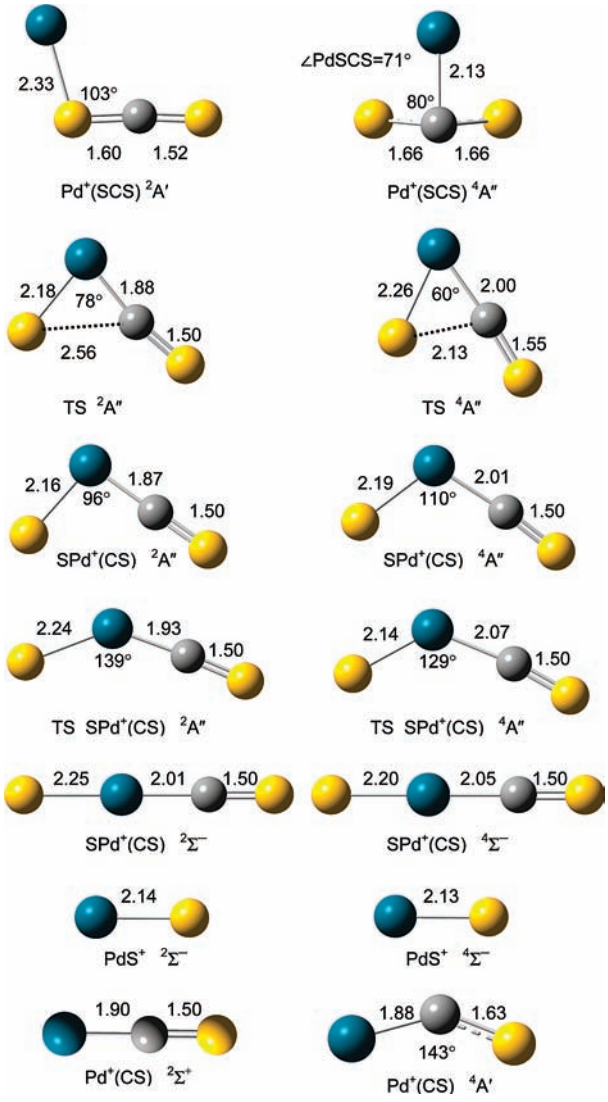

Figure 2. Doublet and quartet spin intermediates, transition states, and products calculated at the B3LYP/Def2TZVPP level of theory and match the order in the reaction coordinate diagram of Figure 1. Bond lengths are shown in Å. All species are planar with the exception of the $^4A''$ state of $Pd^+(SCS)$. Atoms are color-coded as blue for palladium, gray for carbon, and yellow for sulfur.

intermediate that is formed next. Indeed, the geometries of the TS and intermediate are quite similar, Figure 2, consistent with the similarity in the energies, Figure 1 and Table 3. Relaxed potential energy scans, in which the likely reaction coordinate is systematically varied while all other coordinates are allowed to optimize, verify that the transition state connects the two adjacent intermediates. The $SPd^+(CS)$ intermediate has a slightly longer PdS bond compared to the $^2\Sigma^-$ state of the PdS^+ product and a slightly shorter PdC bond compared to the $^2\Sigma^+$ state of the $Pd^+(CS)$ product, Figure 2. The $SPd^+(CS)$ intermediate can be viewed as donation of the σ(CS) lone pair of electrons (the HOMO) into the singly occupied 3σ orbital of PdS^+ ($^2\Sigma^-$). The bent geometry permits a backbonding interaction from a 1δ orbital of PdS^+ to CS, stabilizing the bent configuration compared to a linear geometry, where the π electrons on Pd would be shared with the PdS bond. However, such a linear $SPd^+(CS)$ intermediate (a $^2\Sigma^-$ state) is located only 0.22 eV higher in energy. It can be reached by continuing to increase the SPdC bond angle from 96° in the bent intermediate, passing through a transition state at an angle of 139° and an energy of 0.46 eV above the bent $SPd^+(CS)$ intermediate, Figure 2. Compared to the bent intermediate, the $^2\Sigma^-$ linear intermediate has longer PdS and PdC bonds, Table 3, consistent with sharing of π backbonding electrons.

From either the bent or the linear intermediate, cleavage of the metal ligand bonds can lead to both PdS^+ + CS and $Pd^+(CS)$ + S product channels. If spin is conserved, the accessible product channel for reaction 1 is PdS^+ ($^2\Sigma^-$) + CS ($^1\Sigma^+$), which is an excited state for this channel, Table 1. For reaction 2, the $SPd^+(CS)$ ($^2A''$) ground state intermediate correlates with the $Pd^+(CS)$ ($^2\Sigma^+$) + S (^3P) ground state products.

Note that this reaction path occurs along the $^2A''$ symmetry surface. We also explored whether an equivalent pathway existed having $^2A'$ symmetry as the $Pd^+(SCS)$ intermediate with this symmetry is lower in energy. The $^2A'$ bond insertion transition state lies 0.27 eV above TS($^2A''$) and has a similar geometry. The TS leads to a $SPd^+(CS)$ ($^2A'$) intermediate that lies 0.23 eV higher in energy than the $^2A''$ analogue. Geometries of the two intermediates are quite similar, Table 3. The $^2A'$ intermediate can dissociate to both product channels in the same manner as the $^2A''$ intermediate. Further increase in the SPdC bond angle leads to a $^2A'$ transition state lying 0.77 eV above the analogous $^2A''$ transition state but with a larger angle 157° versus 139° and softer imaginary vibration, 95 versus 233 cm^{-1}, Table 3. The corresponding linear state of $^2\Pi$ symmetry only lies 0.03 eV below the transition state once zero point energies are included (0.02 eV above at the B3LYP level, but 0.03 eV more stable at the B3LYP level before zero point energy corrections). The $^2\Pi$ linear state lies 0.97 eV above the $^2\Sigma^-$ linear intermediate.

We also examined whether the $Pd^+(SCS)$ intermediates might dissociate directly to form PdS^+ + CS products by cleavage of the S−C bond. Calculations indicate that stretching the CS bond in the $^2A'$ intermediate does indeed lead directly to the PdS^+ ($^2\Sigma^-$) + CS ($^1\Sigma^+$) along a surface with no transition state in excess of the product asymptote.

Quartet Potential Energy Surface. Reaction along the quartet surface starts much higher in energy as the ^4F state of Pd^+ is calculated to lie 3.01 eV (3.19 eV experimental) above the ground state. The lowest energy $Pd^+(SCS)$ complex having quartet spin is non-planar, binds the metal to the carbon, and distorts the CS_2 ligand considerably, Figure 2. The CS bond lengths increase from 1.553 to 1.663 Å and the SCS bond angle changes from linear to 123°. This molecule has A″ symmetry with the symmetry plane passing through the PdC bond. This intermediate is bound by 2.23 eV relative to the quartet state asymptote. Lying 0.29 eV higher in energy, Table 3, we locate another $Pd^+(SCS)$ intermediate with $^4A''$ symmetry where the molecule is planar with palladium bridging a CS bond. A $^4A'$ intermediate is found another 0.52 eV higher in energy, but it has an imaginary frequency collapsing it to a lower-energy state.

Oxidative addition of a CS bond to the palladium center leads to the transition state TS($^4A''$), Figure 2, with

Table 3. Geometric Parameters, Vibrational Frequencies, and Relative Energies for Ground State Reactants and Products, and Intermediates and Transitions States for Reaction of Pd^+ with CS_2[a]

species	state	r(Pd−S), Å	r(Pd−C), Å	r(C−S), Å	∠PdSC, deg, ∠SPdC, deg	∠SCS, deg, ∠PdCS, deg	ν, cm^{-1}	E_{rel},[b] eV
$Pd^+ + CS_2$	$^2D + {}^1\Sigma_g^+$			1.553 (2)		180.0 [c]	408 (2), 678, 1561	0.000 (0.000)
Pd^+(SCS)	$^2A'$	2.331		1.599, 1.523	103.1 [c]	175.6 [c]	65, 250, 384, 416, 650, 1516	−1.540 (−1.776)
	$^2A''$	2.321		1.522, 1.604	102.9 [c]	175.0 [c]	62, 227, 372, 408, 642, 1508	−1.230 (−1.477)
	$^4A''$ [d]	2.468 (2)	2.128	1.663 (2)	58.2 (2) [c]	123.3 [c]	119, 137, 275, 315, 757, 956	0.789 (0.597)
	$^4A''$	2.410	2.038	1.706, 1.611	56.3 [c]	125.8 [c]	90, 99, 203, 306, 658, 1023	1.081 (0.700)
TS	$^2A''$	2.179	1.878	1.505, 2.559	45.8,[c] 77.8 [e]	134.1,[c] 169.6 [e]	−175, 180, 272, 338, 413, 1454	−0.075 (−0.102)
	$^2A'$	2.209	1.881	1.510, 2.373	48.3,[c] 70.4 [e]	130.0,[c] 168.7 [e]	−289, 186, 292, 311, 410, 1418	0.192 (0.174)
	$^4A''$	2.257	2.000	1.553, 2.127	54.2,[c] 59.6 [e]	109.3,[c] 175.6 [e]	−389, 168, 194, 217, 336, 1182	1.159 (0.983)
	$^4A'$	2.640	2.159	1.553, 2.207	52.0,[c] 53.6 [e]	116.7,[c] 168.9 [e]	−330, 82, 188, 224, 593, 1126	5.729 (5.298)
SPd^+(CS)	$^2A''$	2.157	1.874	1.502	95.9 [e]	179.5 [e]	73, 264, 266, 354, 391, 1464	−0.076 (−0.139)
	$^4\Sigma^-$	2.205	2.049	1.502	180.0 [e]	180.0 [e]	60 (2), 248, 277 (2), 316, 1440	0.022 (−0.079)
	$^2\Sigma^-$	2.252	2.012	1.503	180.0 [e]	180.0 [e]	55 (2), 258, 272 (2), 293, 1439	0.146 (0.047)
	$^2A'$	2.191	1.875	1.503	87.1 [e]	175.5 [e]	82, 278, 390, 347, 394, 1462	0.157 (0.130)
	$^4A''$	2.188	2.014	1.505	109.7 [e]	174.7 [e]	62, 209, 236, 267, 344, 1422	0.183 (0.130)
	$^4A''$ CP2	2.162	2.123	1.503	114 [e]	175 [e]	43, 201, 213, 218, 374, 1418	0.223 (0.162)
	$^4A''$ CP1	2.149	2.052	1.504	123.5 [e]	174 [e]	−59, 173, 211, 256, 388, 1425	0.225 (0.149)
	$^4A''$ TS	2.139	2.065	1.503	128.6 [e]	173.1 [e]	−82, 165, 215, 253, 399, 1426	0.250 (0.154)
	$^2A''$ CP1	2.245	1.981	1.504	149 [e]	173 [e]	−23, 228, 250, 265, 293, 1430	0.323 (0.192)
	$^2A''$ CP2	2.136	2.209	1.500	105 [e]	177 [e]	−22, 83, 237, 253, 391, 1414	0.367 (0.264)
	$^2A''$ TS	2.240	1.931	1.505	138.9 [e]	176.7 [e]	−233, 137, 249, 254, 320, 1432	0.385 (0.249)
	$^4\Delta$	2.310	2.078	1.501	180.0 [e]	180.0 [e]	50 (2), 234 (2), 255, 296, 1453	(0.877)
	$^2\Pi(^2A')$	2.242	2.031	1.502	180.0 [e]	180.0 [e]	47, 99, 253, 257, 280, 827, 1442	1.120 (1.048)
	$^2A'$ TS	2.215	2.017	1.503	156.9 [e]	177.6 [e]	−95, 175, 237, 245, 280, 1436	1.151 (1.029)
	$^4\Phi$	2.299	2.108	1.500	180.0 [e]	180.0 [e]	60, 65, 244, 246, 269, 309, 1457	(1.704)
	$^4A'$	2.224	1.946	1.643	111.6 [e]	147.5 [e]	−65, 66, 186, 285, 419, 910	4.579 (4.085)
$PdS^+ + CS$	$^4\Sigma^- + {}^1\Sigma^+$	2.133		1.532			393 + 1311	2.116 (2.053)
$Pd^+(CS) + S$	$^2\Sigma^+ + {}^3P$		1.904	1.503		180.0 [e]	247 (2), 330, 1451	1.661 (1.716)

[a] All geometrical parameters are calculated at the B3LYP/Def2TZVPP level of theory. Values in parentheses indicate degeneracies. [b] Relative energies calculated at CCSD(T)/Def2TZVPP//B3LYP/Def2TZVPP (B3LYP/Def2TZVPP) levels of theory, corrected for zero point energies. Absolute calculated energies for the ground state reactants are 960.849503 (962.161631) E_h, including zero point energies. [c] ∠PdSC and ∠SCS. [d] Non-planar with ∠PdSCS = 71°. [e] ∠SPdC and ∠PdCS.

an imaginary frequency of 389 cm^{-1} that again corresponds to the expected CS stretching motion, Table 3. A TS($^4A'$) transition state is located at much higher energies. In this species, the PdS and PdC bond lengths are considerably longer than for TS($^4A''$), consistent with its relative energy. Both transition states go on to form SPd^+(CS) intermediates having the appropriate symmetry. Relaxed potential energy scans verified that the $^4A''$ transition state connects the two adjacent intermediates of $^4A''$ symmetry. The $^4A''$ intermediate has a ∠SPdC bond angle of 110°, a slightly longer PdS bond compared to the $^4\Sigma^-$ state of the PdS^+ product, and a considerably longer PdC bond compared to the $^4A'$ state of the Pd^+(CS) product, Figure 2. Similar to the doublet state, the SPd^+(CS) intermediate can be viewed as donation of the σ(CS) lone pair of electrons into the singly occupied 3σ orbital of PdS^+ ($^4\Sigma^-$), with the bent geometry being stable because of backdonation from the 1δ orbital of PdS^+ into the CS π^* orbitals. However, on the quartet surface, continuing to increase the ∠SPdC bond angle leads to a linear variant of this intermediate that lies lower in energy, by 0.16 eV. The linear SPd^+(CS) intermediate with $^4\Sigma^-$ symmetry has slightly longer PdS and PdC bonds compared to the bent intermediate and substantially longer bonds than the PdS^+ and $PdCS^+$ products because the ligands share π backbonding electrons. The transition state between the bent and linear intermediates lies 0.23 eV above the linear state and has a ∠SPdC bond angle of 129°. In addition to the $^4A''$ bent intermediate, a $^4A'$ state of the SPd^+(CS) intermediate is located. However, it lies very high in energy (4.4 eV above the $^4A''$ state) and has an imaginary frequency of 65 cm^{-1} (an out-of-plane bend) that collapses this structure to the $^4A''$ intermediate. Likewise the linear species has $^4\Delta$ and $^4\Phi$ excited states, which lie 0.96 and 1.78 eV (B3LYP) above the $^4\Sigma^-$ ground state, Table 3.

From either the $^4A''$ or the $^4\Sigma^-$ intermediates, spin-conserving cleavage of the metal ligand bonds can lead to PdS^+ ($^4\Sigma^-$) + CS ($^1\Sigma^+$), the ground state for this channel. Adiabatically, the $^4A''$ and $^4\Sigma^-$ states of the SPd^+(CS) intermediate correlate with the ground state Pd^+(CS) ($^2\Sigma^+$) + S (^3P) asymptote, but spin is also conserved to form Pd^+(CS) ($^4A'$) + S (^3P).

Doublet/Quartet Surface Crossing. As noted above, formation of the ground-state products of reaction 1 from ground-state reactants requires changing spin from doublet to quartet. The efficiency of this spin change is influenced by the extent of spin−orbit coupling (enhanced by the presence of both the heavy metal and sulfur) as well as the character of the seam over which the two spin surfaces interact. To approximate the character of the crossing seam, we take the approach of Yoshizawa et al.[74] Thus, a relaxed potential energy surface scan along a likely region of coordinate space for each spin state is conducted at the B3LYP/Def2TZVPP level of theory, and then the energies of the other spin state at the same geometries are also calculated at the same level of theory. In this system, we examine both the region involving the ∠SPdC bond angle, as well as the dissociation

(74) Yoshizawa, K.; Shiota, Y.; Yamabe, T. *J. Chem. Phys.* **1999**, *111*, 538–545.

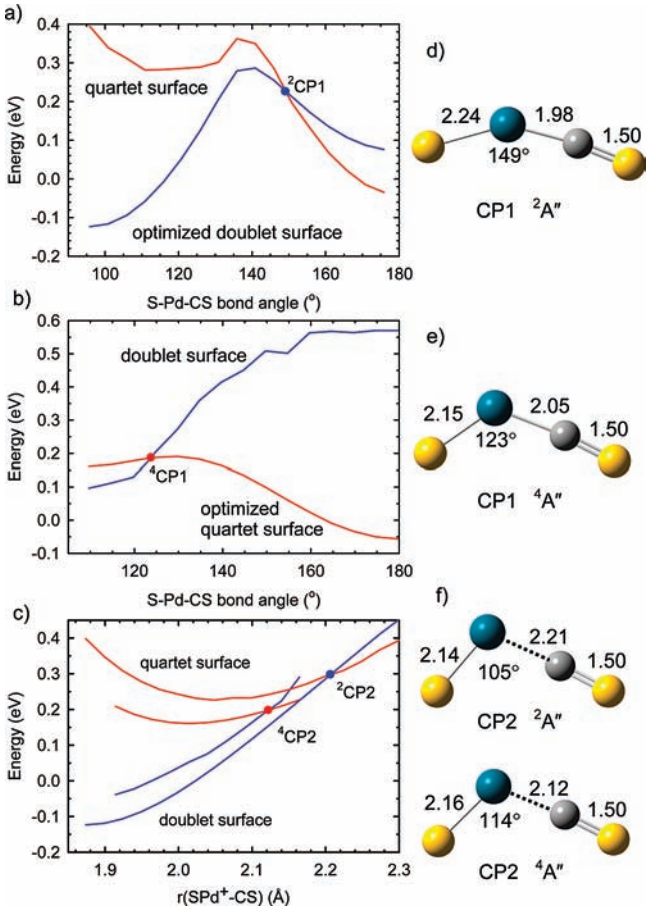

Figure 3. Relaxed potential energy surface scans at the B3LYP/Def2TZVPP level of theory for bending the $SPd^+(CS)$ intermediate (parts a and b) and for stretching the SPd^+-CS bond in the bent intermediates (part c). Results are shown for optimization along the doublet (parts a and c) and quartet (parts b and c) surfaces with single point energies at the same geometries for the other spin state. In part c, the lower energy surface of each spin is the optimized surface. Approximate crossing points (CP) between the surfaces are also indicated by circles with their geometries shown in parts d−f. Bond lengths are shown in Å.

coordinate, that is, stretching the SPd^+-CS bond from both linear and bent intermediates.

The results of these calculations are summarized in Figure 3. Geometries of the approximate crossing points (CPs) are also shown in Figure 3, with their energies calculated at both the CCSD(T) and B3LYP levels listed in Table 3. Along the optimized doublet surface for bending, Figure 3a, the ^{2}CP1 crossing point occurs just past the transition state at a ∠SPdC bond angle of 149° and an energy of 0.32 eV, Table 3. Along the optimized quartet surface, Figure 3b, ^{4}CP1 lies just before the transition state at a bond angle of 123° and an energy of 0.23 eV. Given the shallowness of the potential energy surface along the bending coordinate, Figure 1, it seems likely that there is a fairly broad seam over which the two spin surfaces interact for the bending coordinate.

When the reaction coordinate for SPd^+-CS bond dissociation is examined (not shown), we find that the surfaces evolving from the linear intermediates do not cross at all (or rather the crossing occurs at *shorter* bond distances of about 1.6 Å), consistent with the fact that the quartet spin states of the linear intermediate and the product asymptote are lower than the doublet surface,

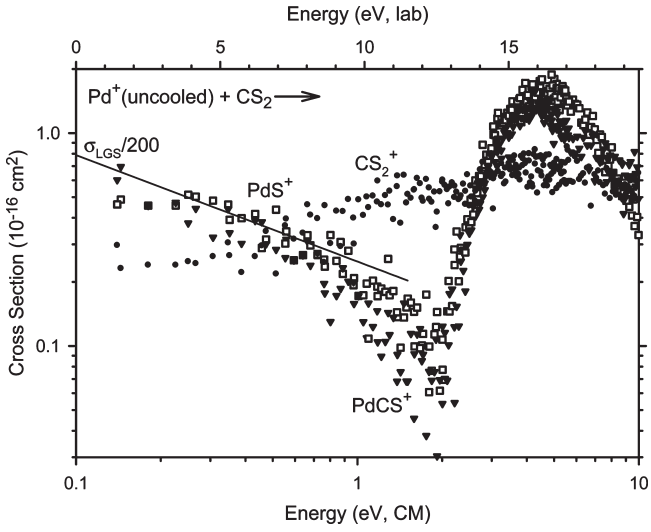

Figure 4. Product cross sections for the reaction of uncooled Pd^+ with CS_2 to form PdS^+ (open squares), $PdCS^+$ (inverted triangles), and CS_2^+ (circles) as a function of center of mass energy (lower axis) and laboratory energy (upper axis).

Figure 1. For dissociation from the bent doublet intermediate, ^{2}CP2 lies at 2.21 Å and an energy of 0.37 eV, and along the quartet surface, ^{4}CP2 lies at 2.12 Å and an energy of 0.23 eV, Figure 3c.

There should also be a surface crossing along the dissociation asymptote forming $PdS^+ + CS$ directly from the $Pd^+(SCS)$ intermediates, Figure 1. Although this crossing was not explicitly examined computationally, the distinct energies of the doublet and quartet states of this intermediate suggest that the crossing will occur late along the dissociation pathway. Thus, it seems unlikely that spin-inversion along this coordinate will be efficient.

Experimental Results

Reaction of Pd^+ with CS_2 yields two major products, PdS^+ and $PdCS^+$, formed in reactions 1 and 2, along with the charge transfer product ion, CS_2^+. Unlike the flow tube studies of Bohme and co-workers,[35] no $Pd^+(CS_2)$ adducts are observed because the single collision conditions used here do not allow the collisional relaxation necessary to form such adducts. Figure 4 depicts the results obtained for Pd^+ ions produced using the DC discharge with no quenching gases added to the flow tube. It can be seen that the PdS^+ and $PdCS^+$ cross sections have nearly identical magnitudes and decline at the lowest energies reaching minima at about 2 eV before rising again at higher collision energies. Thus both reactions take place via a barrierless, exothermic pathway, as well as a more intense endothermic pathway. The energy dependence of the low energy feature is consistent with the Langevin−Gioumousis−Stevenson (LGS) collision cross section for ion−molecule reactions,[75] $\sigma_{LGS}(E) = (\pi q/4\pi\varepsilon_0)(2\alpha/E)^{1/2}$, where q is the charge on the ion, ε_0 is the permittivity of vacuum, E is the collision energy, and α is the polarizability of CS_2, 8.74 Å^3.[76] The charge transfer reaction has a finite cross section at low energies, rises slowly with increasing energy, until it reaches a magnitude that changes little above about 1.5 eV. The ionization energies of

(75) Gioumousis, G.; Stevenson, D. P. *J. Chem. Phys.* **1958**, *29*, 294.
(76) Miller, T. M.; Bederson, B. *Adv. At. Mol. Phys.* **1977**, *13*, 1.

CS_2 and Pd are 10.073 ± 0.005[77] and 8.3369 ± 0.0001 eV,[78] respectively, such that the charge transfer reaction involving ground states species is endothermic by 1.736 ± 0.005 eV. Therefore, observation of this reaction at low energies indicates that excited states of the Pd^+ cation must be present. The lowest energy excited state is the $^2D_{3/2}$ spin−orbit level, which lies only 0.44 eV above the $^2D_{5/2}$ ground state, whereas the next excited state of Pd^+, $^4F_{9/2}$, lies 3.11 eV above the $^2D_{5/2}$ ground state level.[73] Therefore, the excited species responsible can be any excited state except the $^2D_{3/2}$ level and is likely to be primarily the ^4F state, the lowest-lying quartet state. On the basis of the magnitude of the PdS^+ and $PdCS^+$ cross sections compared to σ_{LGS}, Figure 4, the population of these excited states could be as little as 1% of the reactant ion beam (which assumes that they react with 100% efficiency).

The presence of excited states is confirmed by admitting small amounts of CS_2 into the flow tube to quench the excited states, which clearly react exothermically with neutral CS_2. When the Pd^+ cations are formed in this fashion, the magnitudes of the CS_2^+ cross section and those of the exothermic features in the PdS^+ and $PdCS^+$ cross sections all decrease by about 1 order of magnitude, whereas the endothermic features in the latter cross sections decline only by about 20%. Unfortunately, no flow tube conditions could be found that eliminated the features associated with excited states of Pd^+. Therefore, cross sections associated with the reactions of ground state Pd^+ (^2D) are determined by extrapolating the cross sections for unquenched and quenched Pd^+ to remove the excited-state features, essentially by scaling the unquenched data down to match the magnitude of the excited-state feature in the quenched data, subtracting, and then rescaling the remainder to properly reflect 100% Pd^+(^2D). The resulting extrapolated cross sections are shown in Figure 5. Because of the distinct energy dependence of the excited-state features and their small magnitude (especially in the quenched data), the thermochemical results obtained below are not influenced by this extrapolation procedure.

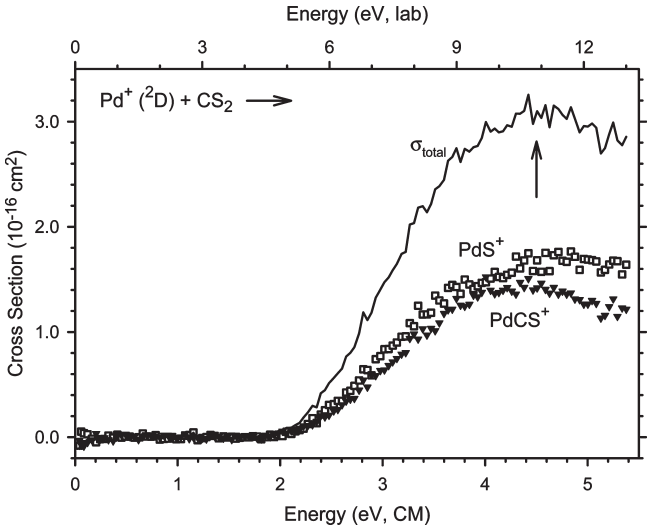

Figure 5. Extrapolated product cross sections for the reaction of Pd^+(^2D) with CS_2 to form PdS^+ (open squares), $PdCS^+$ (closed inverted triangles), and their sum (line) as a function of center-of-mass energy (lower axis) and laboratory energy (upper axis). The arrow marks D_0(S−CS) = 4.50 eV.

The PdS^+ and $PdCS^+$ cross sections rise from apparent thresholds near 2 eV. Above about 4.5 eV, both cross sections can decline because of the dissociation of the products, the overall process (eq 6), which starts at D_0(SC−S) = 4.50 ± 0.04 eV.[72]

$$Pd^+ + CS_2 \rightarrow Pd^+ + CS + S \qquad (6)$$

Careful analysis of the threshold regions for the cross sections of reactions 1 and 2 using eq 3 yields the E_0, σ_0, and n values summarized in Table 4. Initial analysis is performed by analyzing the reaction channels independently. Although reaction 1 has a slightly larger cross section, the threshold energies for the two channels are similar but smaller for reaction 2 (by ~0.03 eV).

The PdS^+ and $PdCS^+$ channels are also analyzed as competitive reactions assuming that the EM is the ground state SPd^+(CS) intermediate with an energy relative to the reactants calculated at the CCSD(T)//B3LYP level. Assuming loose (PSL) transitions states for formation of both products and return to reactants, eq 4 is able to reproduce the data nicely throughout the threshold region, up to 4.5 eV, where reaction 6 can begin, as shown in Figure 6. The model reproduces the shapes of both the PdS^+ and the $PdCS^+$ cross sections well, even though the energy dependences are slightly different and despite the fact that the value of n used is the same for both channels in the competitive analysis. Conventionally, the value of the parameter m in eq 4 is held to unity, however, here values of m = 1.0 and 1.5 are both tried and yield very similar fits, with nearly identical threshold energies. As discussed previously for the reaction of V^+ with CS_2,[22] spin inversion can change the cross-section shape. Because more energetic reactants pass through the surface-crossing region more rapidly, the ability of the electrons to adjust to

Table 4. Summary of Parameters in Equations 3 and 4 Used to Analyze the Cross Sections for Reactions 1 and 2[a]

reaction	σ_0	n	m	E_0, eV	$D_0(Pd^+-X)$, eV
$Pd^+ + CS_2 \rightarrow PdS^+ + CS$	3.5 (0.7) [b]	0.9 (0.1)	1.0	2.46 (0.04)	2.04 (0.06)
	2.2 (0.9) [c]	1.3 (0.3)	1.0	2.13 (0.08)	2.37 (0.11)
	2.7 (1.3) [c]	1.7 (0.4)	1.5	2.14 (0.08)	2.36 (0.11)
	2.5 (0.9) [d]	1.2 (0.3)	1.0	2.14 (0.07)	2.36 (0.11)
	2.5 (0.8) [d]	1.7 (0.3)	1.5	2.14 (0.07)	2.36 (0.11)
$Pd^+ + CS_2 \rightarrow PdCS^+ + S$	2.5 (0.9) [b]	1.0 (0.3)	1.0	2.43 (0.13)	2.07 (0.14)
	11.0 (4.8) [c]	1.3 (0.3)	1.0	1.92 (0.09)	2.58 (0.12)
	13.0 (6.7) [c]	1.7 (0.4)	1.5	1.92 (0.08)	2.58 (0.12)
	58 (25) [d]	1.2 (0.3)	1.0	1.74 (0.09)	2.76 (0.12)
	55 (23) [d]	1.7 (0.3)	1.5	1.74 (0.09)	2.76 (0.12)

[a] Uncertainties in parentheses. Values for E_0 are two standard deviations. [b] Single channel fit using eq 3. [c] Competitive fit using eq 4 with a loose (PSL) transition state for reaction 2. [d] Competitive fit using eq 4 with a tight transition state for reaction 2.

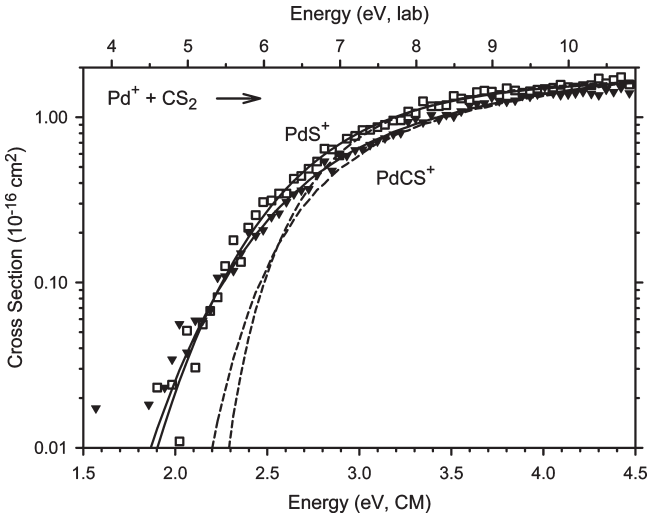

Figure 6. Cross sections for the reaction of Pd^+ with CS_2 to form PdS^+ (open squares) and $PdCS^+$ (closed inverted triangles) as a function of center-of-mass energy (lower axis) and laboratory energy (upper axis). Solid lines show the competitive model cross sections given by eq 4 and the parameters given in Table 4 ($m = 1.0$). Dashed lines show these models in the absence of experimental kinetic energy distributions for reactants at 0 K.

different configurations along the reaction coordinate is reduced. Thus, a spin-forbidden path can exhibit a reaction efficiency that varies approximately as $E^{-1/2}$, which can be included in the data analysis by using a value of 1.5 for the parameter m. Because reaction 1 is spin-forbidden, this alternate value of m is included in the present data analysis.

It is possible that the formation of $PdS^+ + CS$ and $PdCS^+ + S$ from the $SPd^+(CS)$ intermediate have different types of transition states because the former process involves the cleavage of a donor−acceptor bond whereas the latter process cleaves a covalent bond. Therefore, it is possible that the latter process is more accurately described by a tight transition state, as found elsewhere for covalent bond cleavages.[54,55] When the data are competitively modeled using a transition state in which the vibration corresponding to the reaction coordinate is removed and all other rovibrational parameters are maintained at the values for the intermediate, which is the tightest realistic transition state for a barrierless dissociation, we find that the data are again reproduced well. The threshold energy for reaction 1 is unchanged from the value obtained when both channels have PSL transition states, but that for reaction 2 drops by 0.18 eV, consistent with a larger kinetic shift associated with the tight transition state.

The competitive analysis yields thresholds for the two reactions that are more distinct, Table 4, with that for $PdCS^+$ being lower by 0.22 ± 0.03 eV (0.40 ± 0.03 eV when a tight transition state is assumed). The competitive analysis thresholds are lower than those from the independent analysis because of the effects of competition with channels leading back to reactants, the only available pathway at low energies. Even though the $PdCS^+$ cross section has a lower threshold, it remains slightly smaller than the PdS^+ cross section (except at the very lowest energies). Furthermore, the fit shown requires that the $PdCS^+$ channel be scaled up by a factor of 4.8 ± 1.3 (as reflected by the different σ_0 values in Table 4). This scaling is needed because the $PdS^+ + CS$ channel has 4 rotational and 2 vibrational degrees of freedom whereas the $PdCS^+ + S$ channel has 2 rotations and 4 vibrations, such that the former channel is greatly favored by the number of available states. The scaling factor can be rationalized by the differences in the electronic degeneracies of the two channels: 4 for the PdS^+ ($^4\Sigma^-$) + CS ($^1\Sigma^+$) channel versus 18 for the $Pd^+(CS)$ ($^2\Sigma^-$) + S (^3P) channel, which introduces a scaling factor of 4.5, in good agreement with that empirically found. The fact that the latter channel can be formed with no spin change may also influence its probability compared with the spin-forbidden formation of PdS^+. In this regard, we also analyzed the data assuming that the spin-allowed PdS^+ ($^2\Sigma^-$) product is formed instead. The fitting parameters of eq 4 remain comparable to those obtained for the $^4\Sigma^-$ state with thresholds changing by less than 0.01 eV. This is because the molecular parameters of the two states are very similar, Table 1. For these products, the ratio of electronic degeneracies for reactions 1 and 2 is now 2 versus 18, or a factor of 9, larger than the scaling factor obtained experimentally, which suggests that the experimental data is more consistent with formation of the PdS^+ ($^4\Sigma^-$) ground state.

When the data are analyzed assuming a tight transition state for reaction 2, a scaling factor of 23.6 ± 8.5 is required to reproduce the data. It is difficult to rationalize such a large scaling factor, which suggests that this transition state is much too tight. Finally, we note that the value of n used in these competitive fits is near unity when $m = 1.0$, a conventional line-of-centers value. When $m = 1.5$, the value of n rises by a comparable amount, 0.4, compensating for the change in the energy dependence. Overall, there is no clear indication that the extra value of $E^{-1/2}$ is needed, but the final threshold results are essentially independent of this parameter.

Finally, it is also possible that the $PdS^+ + CS$ channel is favored compared to $Pd^+(CS) + S$ formation because the former can be produced directly from the initially formed $Pd^+(SCS)$ intermediate, without the need for bond insertion. Such an alternate pathway could increase the probability of reaction 1 relative to reaction 2, which could also contribute to the scaling factors found empirically. Analysis of the data explicitly including such a possibility is beyond the capability of the analysis software; however, the presence of this alternative pathway does not change the fact that the two channels are still coupled. Because the rates of reaction are most sensitive to the number of states at the transition state and relatively insensitive to the density of states of the EM, eq 5, the competition between reactions 1 and 2 relies primarily on the properties of the products. As these properties are explicitly accounted for in the competitive analysis above, the presence of this additional pathway is unlikely to change the thermodynamics obtained.

The E_0 values extracted from analysis of the data can be converted to Pd^+-S and Pd^+-CS bond strengths at 0 K using eq 7, where X can represent either S or CS. These values are also provided in Table 4.

$$D_0(Pd^+ - X) = D_0(SC - S) - E_0 \quad (7)$$

It can be seen that the values obtained from the competitive

(77) Lias, S. G. *Ionization Energy Evaluation in NIST Chemistry WebBook, NIST Standard Reference Database Number 69*; Linstrom, P. J.; Mallard, W. G., Eds.; National Institute of Standards and Technology: Gaithersburg, MD; http://webbook.nist.gov (accessed June 24, 2009).

(78) Callender, C. L.; Hackett, P. A.; Rayner, D. M. *J. Opt. Soc. Am. B* **1988**, *5*, 614.

Table 5. Experimental and Theoretical Bond Energies (eV)

bond	exp	B3LYP[a]	CCSD(T)//B3LYP[a]	CCSD(T)//CCD[a]	CCSD(T)[a]
Pd^+-S	2.36 ± 0.11	2.636 (2.646)	2.119 (2.239)	2.035 (2.133)	2.143 (2.267)
Pd^+-CS	2.67 ± 0.21	2.979 (2.984)	2.551 (2.694)	2.505 (2.631)	2.617 (2.751)
MAD[b]		0.29 ± 0.02	0.18 ± 0.09	0.24 ± 0.11	0.14 ± 0.12

[a] In all cases, theoretical values are obtained at the level shown using the Def2TZVPP basis set. Values are corrected for zero point energies and for basis set superposition errors in the full counterpoise limit. Values without counterpoise corrections are in parentheses. [b] Mean absolute deviation from experimental values.

modeling are slightly higher than those obtained from the independent analyses, where the latter have been reported previously.[31] We believe that the more sophisticated competitive modeling, which reproduces both cross sections simultaneously, provides the most accurate threshold values in addition to being more precise. Our best values are taken as the average of the competitive fits using $m = 1.0$ and 1.5 as well as the loose (PSL) and tight transition state assumptions for reaction 2: $D_0(Pd^+-S) = 2.36 \pm 0.11$ eV and $D_0(Pd^+-CS) = 2.67 \pm 0.21$ eV, where the uncertainties are two standard deviations. Uncertainties include variations among the TS assumptions and values of m, multiple data sets (seven), frequencies of reactants and products (±10%), time available for reaction (factor of 2), absolute energy of the EM (±0.3 eV), and the uncertainty in the absolute zero of energy (±0.02 eV).

Discussion

Thermochemistry. After correcting for basis set superposition errors (BSSE) at the full counterpoise limit,[79,80] the calculated bond energy of the PdS^+ ($^4\Sigma^-$) ground state is 2.64 eV at the B3LYP level of theory, considerably higher than the 2.12, 2.04, and 2.14 eV values calculated at the CCSD(T)//B3LYP, CCSD(T)//CCD, and CCSD(T) levels of theory, respectively, Table 5. These values bracket the experimental bond energy of 2.36 ± 0.11 eV, with discrepancies comparable to those of the calibration calculations. Further, a similar discrepancy (0.24−0.29 eV) is found in the case of RhS^+ compared to the CCSD(T) bond energies.[34] Because of spin-conservation in the exit channel, as noted above, it is possible that the experimental threshold corresponds to formation of the PdS^+ ($^2\Sigma^-$) excited state. This species has calculated bond energies of 2.41 eV (B3LYP), 1.94 eV (CCSD(T)//B3LYP), 1.83 eV (CCSD(T)//CCD), and 1.84 eV (CCSD(T)). Now the B3LYP value agrees with experiment, but the presumably more accurate CCSD(T) values are much too low. Overall, we believe these results suggest that ground-state PdS^+ is formed experimentally and indicate that spin need not be conserved in this reaction. The relaxation of spin conservation is by no means unusual under such reaction conditions and has been observed in many other transition metal systems,[21−29,32−34,81−85] including the lighter congener of Pd^+, Ni^+ reacting with CS_2.[28]

For the palladium thiocarbonyl cation, the ground state is bound by 2.98, 2.55, 2.50, and 2.62 eV at the B3LYP, CCSD(T)/B3LYP, CCSD(T)/CCD, and CCSD(T) levels of theory, respectively, with counterpoise corrections. The latter values are in good agreement with the experimental value of 2.67 ± 0.21 eV. Here, there are no spin restrictions in the formation of any of the $PdCS^+$ states. Note that theory indicates that the Pd^+-CS bond is stronger than the Pd^+-S bond by 0.34−0.47 eV (Table 5), whereas experiment finds differences of 0.03−0.40 eV, with the upper value obtained with the tight transition state assumption for reaction 2. It should be noted that the metal−ligand bonding in these two molecules is quite distinct, covalent and dative, respectively, such that theory may not provide balanced views of both interactions.

In addition, the spin−orbit interactions in these product ions may differ appreciably. Experimental bond energies refer to the ground spin−orbit state at 0.0 eV, $^2D_{5/2}$ for Pd^+. In contrast, calculations are referenced to the statistically weighted mean of all spin−orbit levels in the ground-state term, 0.18 eV for Pd^+ (^2D).[73] Because our calculations do not explicitly include spin−orbit interactions, it is possible that calculated bond energies should be reduced by this different asymptotic energy before comparison with experimental values. However, spin−orbit effects influence the energetics of all reactants, intermediates, and products with unknown magnitudes. For example, the spin−orbit splitting of ground-state RhS ($^4\Sigma^-$) has been measured as only 0.006 eV.[86] Because of these unknown splittings, we do not apply corrections in the present work, which implicitly assumes that the spin−orbit corrections largely cancel, which would appear to be the case for $PdCS^+$ but not PdS^+.

Reaction Mechanism. The reaction coordinate diagram of Figure 1 shows clearly that reactions 1 and 2 can occur by insertion of the palladium cation into a CS bond of CS_2 followed by simple cleavage of one of the metal ligand bonds. Reaction 1 can also occur directly from the initially formed Pd^+(SCS) intermediate by C−S bond cleavage. The experimental results correspond to reaction of ground state Pd^+(^2D), which the calculations indicate can form the ground state Pd^+(CS) ($^2\Sigma^+$) + S (^3P) products by remaining on the doublet surface throughout the reaction. In contrast, formation of the ground state PdS^+ ($^4\Sigma^-$) + CS ($^1\Sigma^+$) products clearly requires a change in spin. As discussed above, the spin crossing occurs in the

(79) Boys, S. F.; Bernardi, R. *Mol. Phys.* **1970**, *19*, 553.
(80) van Duijneveldt, F. B.; van Duijneveldt de Rijdt, J. G. C. M.; van Lenthe, J. H. *Chem. Rev.* **1994**, *94*, 1873.
(81) Elkind, J. L.; Armentrout, P. B. *J. Phys. Chem.* **1986**, *90*, 5736–5745.
(82) Schultz, R. H.; Elkind, J. L.; Armentrout, P. B. *J. Am. Chem. Soc.* **1988**, *110*, 411–423.
(83) Armentrout, M. M.; Li, F.-X.; Armentrout, P. B. *J. Phys. Chem. A* **2004**, *108*, 9660–9672.
(84) Parke, L. G.; Hinton, C. S.; Armentrout, P. B. *Int. J. Mass Spectrom.* **2006**, *254*, 168–182.
(85) Li, F.-X.; Zhang, X.-G.; Armentrout, P. B. *Int. J. Mass Spectrom.* **2006**, *255*/*256*, 279–300.
(86) Li, R.; Balfour, W. J.; Hopkins, W. S.; Adam, A. G. *J. Mol. Spectrosc.* **2005**, *234*, 211–215.

vicinity of the $SPd^+(CS)$ intermediate and appears to primarily involve the SPdC bending coordinate. Therefore, it seems likely that appreciable time is available to permit spin−orbit coupling between the doublet and quartet surfaces, such that spin conservation is not required. This conclusion is consistent with the good agreement between the experimental bond energy for PdS^+ and that obtained theoretically for the $^4\Sigma^-$ ground state.

Summary

The gas-phase reactivity of the late atomic transition metal cation, Pd^+, with CS_2 has been investigated using GIB tandem mass spectrometry and theoretical calculations. Careful analysis and evaluation of the threshold energies, reactivities, and cross sections results in bond dissociation energies of the palladium sulfide cation, $D_0(Pd^+-S) = 2.36 \pm 0.11$ eV, and the palladium thiocarbonyl cation, $D_0(Pd^+-CS) = 2.67 \pm 0.21$ eV. These bond energy values agree reasonably well with theoretical values at the CCSD(T)/Def2TZVPP//B3LYP/Def2TZVPP, CCSD(T)/Def2TZVPP//CCD/Def2TZVPP, and CCSD(T)/Def2TZVPP levels of theory, whereas B3LYP/Def2TZVPP calculations tend to overbind. Residual discrepancies between experiment and theory may be related to differences in the spin−orbit splitting of the molecular species relative to atomic Pd^+.

Calculations of the potential energy surfaces for these reactions clearly indicate that insertion of the palladium cation into a CS bond of CS_2 is required. Loss of either ligand then leads to ground state products. Mixing of the doublet and quartet spin states in the vicinity of the $SPd^+(CS)$ intermediate appears to be facile such that spin conservation is not required in this system.

Acknowledgment. Profs. D. Schröder and H. Schwarz are thanked for their support and guidance when these data were taken. This work was supported by the Fonds der Chemischen Industrie and the National Science Foundation (P.B.A., CHE-0748790). In addition, we thank the Center for High Performance Computing at the University of Utah for the generous allocation of computer time. A referee is thanked for suggesting the alternative reaction pathway discussed above.